AIAA JOURNAL
Vol. 51, No. 5, May 2013

Classical, Refined, and Component-Wise Analysis of Reinforced-Shell Wing Structures

E. Carrera,* A. Pagani,† and M. Petrolo‡
Politecnico di Torino, 10129 Turin, Italy

DOI: 10.2514/1.J052331

This paper compares early and very recent approaches to the static analysis of reinforced-shell wing structures. Early approaches were those based on the pure semimonocoque theory along with the beam assumptions of the Euler–Bernoulli and Timoshenko type. The recent approaches are based on a hierarchical, one-dimensional formulation. These are obtained by adopting various polynomial expansions of the displacement field above the cross-section of the structure according to the unified formulation which was recently proposed by the first author. Two classes were developed in the unified formulation framework. In the first class, Taylor expansion models were developed by exploiting *N*-order Taylor-like polynomials; classical beam theories (Euler–Bernoulli and Timoshenko) were obtained as special cases of Taylor expansion. In the second class, Lagrange expansion models were built by means of four- and nine-point Lagrange-type polynomials over the cross-section of the wing. The component-wise approach was obtained by using different four- and nine-point Langrangian descriptions for different wing components including panels, ribs, spar caps, stringers, and transverse ribs. The finite element method was used to develop numerical applications in the weak form. Finite element matrices and vectors are expressed in terms of fundamental nuclei whose forms do not formally depend on the order and the expansion. A number of typical aeronautical structures were analyzed, and semimonocoque results were compared to classical (Euler–Bernoulli and Timoshenko), refined (Taylor expansion), and component-wise (Lagrange expansion) models. Stress and displacement fields of simple statically determinate, redundant, and open-section wing-box structures were analyzed. Finite element models by a commercial software that make use of solid and shell elements were used for comparison purposes. Results have highlighted the enhanced capabilities of the present refined and component-wise formulations. The present component-wise approach appears to be the natural tool to analyze wing structures because it leads to results that can only be obtained by the use of three-dimensional elasticity (solid) elements whose costs are at least one order of magnitude higher than component-wise cases. Component-wise models in conjunction with finite elements could be seen as a modern way of analyzing reinforced-shell structures by removing classical assumptions of constant shear in the spar webs and panels.

Nomenclature

$\tilde{C}_{ij}$	=	material coefficients
$\tilde{\boldsymbol{C}}_{pp}$, $\tilde{\boldsymbol{C}}_{pn}$, $\tilde{\boldsymbol{C}}_{np}$, $\tilde{\boldsymbol{C}}_{nn}$	=	material stiffness subarrays
$\boldsymbol{D}_p$, $\boldsymbol{D}_{np}$, $\boldsymbol{D}_{ny}$	=	differential operator matrices
E	=	Young's modulus
F_s	=	cross-section function of the variation
F_τ	=	cross-section function of the variable
G	=	shear modulus
$\boldsymbol{K}^{ij\tau s}$	=	fundamental nucleus of the stiffness matrix
L	=	dimension of the structure in the y direction
L_{ext}	=	external work
L_{int}	=	internal work
N	=	order of the expansion above the cross-section for the Taylor expansion models
N_i	=	shape function of the variable
N_j	=	shape function of the variation
$\boldsymbol{q}$	=	nodal displacement vector
$\boldsymbol{u}$	=	displacement vector
u_x, u_y, u_z	=	displacement components in the x, y, and z directions
x, y, z	=	coordinate reference system
δ	=	virtual variation
ϵ	=	strain vector
ν	=	Poisson's ratio
$\boldsymbol{\sigma}$	=	stress vector
Ω	=	cross-section domain

Received 12 September 2012; revision received 11 December 2012; accepted for publication 19 December 2012; published online 25 March 2013.

*Professor of Aerospace Structures and Aeroelasticity, Department of Mechanical and Aerospace Engineering, Corso Duca degli Abruzzi 24; erasmo.carrera@polito.it. Member AIAA (Corresponding Author).

†Ph.D. Student, Department of Mechanical and Aerospace Engineering, Corso Duca degli Abruzzi 24; alfonso.pagani@polito.it.

‡Research Assistant, Department of Mechanical and Aerospace Engineering, Corso Duca degli Abruzzi 24; marco.petrolo@polito.it.

I. Introduction

PRIMARY aircraft structures are essentially reinforced thin shells [1]. These are so-called semimonocoque constructions, which are obtained by assembling three main components: skins (or panels), longitudinal stiffening members (including spar caps), and transversal stiffeners (ribs). The determination of stress/strain fields in these structural components is of prime interest for structural analysts. Many different approaches were developed in the first half of the last century. These are discussed in major reference books [1,2] and more recently in [3]. Among these approaches, pure semimonocoque (PS), or idealized semimonocoque, is the most popular because it assumes constant shear into panels and shear webs. The main advantage of PS is that it leads to a system of linear algebraical equations. However, the number of such equations rapidly increases for multi-bay box structures with high redundancy. The number of resulting equations (and redundancy) can be strongly reduced by coupling PS with assumptions from Euler–Bernoulli beam theory (EBBT) or Timoshenko beam theory (TBT). Many works are known to overcome limitations related to constant shear hypotheses; see [4–8] as examples. The systematic use of matrix methods in aircraft structure analysis was introduced by Argyris and Kensley [9]. Here, the PS approach and force methods were used to describe an automatic technique to build compliance matrices. This automatic

technique is one of the pioneering contributions to the development of finite element methods (FEMs).

Because of the advent of computational methods, mostly FEM, the analysis of complex aircraft structures continued to be made using a combination of solids (three-dimensional), plates/shells (two-dimensional), and beams (one-dimensional). These were implemented first in NASTRAN codes. Many other commercial FE codes have been developed and used in aerospace industries. Nowadays, FEM models with a number of unknown degrees of freedom (DOFs) close to 10^6 are widely used in common practise. The possible manner in which stringers, spar caps, spar webs, panels, and ribs are introduced into FE mathematical models is part of the knowledge of structural analysts. A short discussion of this follows. A number of works have shown the necessity for a proper simulation of the stiffener-panel "linkage". Satsangi and Murkhopadhyay [10] used eight-node plate elements assuming the same displacement field for stiffeners and plates. Kolli and Chandrashekhara [11] formulated an FE model with nine-node plate and three-node beam elements. Gangadhara Prusty [12] carried out linear static analyses of composite laminated shells using a combination of eight-node plate elements and three-node beam elements. Recently, Thinh and Khoa [13] have developed a new nine-node rectangular plate model to study the free vibrations of shell structures with arbitrary oriented stiffeners. It is often necessary to model stiffeners out of the plate/shell element plane. In this case, beam nodes are connected to the shell element nodes via rigid fictitious links. This methodology presents some inconsistencies. The main problem is that the out-of-plane warping displacements in the stiffener section are neglected, and the beam torsional rigidity is not correctly predicted. Several solutions have been proposed in the literature to overcome this issue. Patel et al. [14] introduced a torsion correction factor. Vörös [15,16] proposed a procedure to model the connection between the plate/shell and the stiffener where the shear deformation of the beam is neglected and the formulation of the stiffener is based on the well-known Bernoulli–Vlasov [17] theory. In Vörös's method [15,16], the stiffener element has two nodes with 7 DOFs per node. To maintain the displacement compatibility between the beam and the stiffened element, a special transformation was used, which included torsional-bending coupling and the eccentricity of internal forces between the stiffener and the plate elements. Three-dimensional (3-D) finite element models are usually implemented as soon as the wing's structural layouts are determined. Because of their complexity, solid models are commonly used only within optimization procedures. In fact, despite the availabilities of even cheaper computer power, these FEM models present large computational costs, and their use in a multifield iterative process, such as in an aeroelastic analysis, is quite a burden. Nowadays, the trend is to use equivalent, simplified, lower-fidelity, one-dimensional (1-D) FEM models (the so-called stick-model) of the wing structure to be used within iterative algorithms. There are numerous papers dealing with wing stick models in the literature, such as [18–20]. These methodologies are based on the extraction of the structural stiffness of the wing with respect to its principal axes. Those stiffness properties are then employed to generate the wing stick model. Simplified models are generally created along the wing's elastic axis. This applies a geometrical constraint so that the stick model principal torsional axis acts as the wing elastic axis. It could be concluded that the development of computationally cheaper models compared to those by standard FE models, but with high accuracy, still plays a crucial role in aircraft structure analysis.

The present work falls in the framework of the Carrera unified formulation (CUF), which has been developed during the last decade by the first author and his coworkers. CUF was initially devoted to the development of refined plate and shell theories; see [21,22]. In recent works [23,24], CUF has been extended to beam modeling. Two classes of 1-D CUF models were proposed: the Taylor expansion (TE) class and the Lagrange expansion (LE) class. TE models exploit N-order Taylor-like polynomials to define the displacement field above the cross-section with N as a free parameter of the formulation. Static [25,26] and free-vibration analyses [27,28] showed the strength of 1-D CUF models in dealing with arbitrary geometries, thin-walled structures, and local effects. Moreover, asymptotic-like analyses leading to reduced refined models were carried out [29]. The EBBT and TBT are derived from the linear Taylor-type expansion. The LE class is based on Lagrange-like polynomials to discretize the cross-section displacement field. LE models have only pure displacement variables. Static analyses on isotropic [30] and composite structures [31] revealed the strength of LE models in dealing with open cross-sections and arbitrary boundary conditions as well as obtaining layer-wise descriptions of the 1-D model.

The present paper proposes a CUF-based approach in the analysis of complex wing structures. A number of significant problems dealing with reinforced-shell structures are addressed in the following sections. Classical, refined, and component-wise (CW) models are implemented for different structural configurations. Particular attention is given to the CW approach. Component-wise means that each typical component of a reinforced-shell structure (i.e., stringers, sheet panels, and ribs) can be modeled by means of a unique 1-D formulation. The CW approach has recently been exploited for the analysis of laminated composites [32], and it has proven to be able to model single fibers and related matrices, entire layers, and whole multilayers. In the present work, the CW approach is presented as an efficient way of dealing with the static analysis of reinforced-shell wing structures.

The paper is organized as follows. A brief description of the models adopted is given in Sec. II; advanced beam theories based on CUF are described in Sec. III, together with the finite element formulation; numerical results are provided in Sec. IV; and main conclusions are then outlined in Sec. V.

II. Description of the Considered Structural Models

A brief description of the models used in the present paper is provided herein. First, analytical approaches are drawn. Refined and CW as well as classical beam theories are then introduced by means of 1-D CUF, which is described in Sec. III.

A. Pure Semimonocoque

These models are based on the simplifying assumptions of the semimonocoque assembled components, as described in Sec. I. Stringers are here considered as concentrated areas carrying only axial stresses, whereas webs and panels carry only shearing stresses. According to [1–3], the internal loads in a statically determinate reinforced-shell structure can be found by the use of static equilibrium equations alone. In a statically indeterminate structure, additional equations along with the static equilibrium equations are necessary to find all the internal stresses. In such a case, we should impose compatibility conditions to deal with redundant forces and stresses. These conditions can be written in various forms by applying elasticity theorems; among these, the principle of virtual displacements (PVD) is used in this article as in [2,3]. This approach is hereafter referred to as the pure semimonocoque (PS) model.

B. Beam Semimonocoque

The classical and best-known beam theories are EBBT [33] and TBT [34]. The former does not account for transverse shear deformations. The latter foresees a uniform shear distribution along the cross-section of the beam. For instance, referring to the coordinate frame shown in Fig. 1, the displacement components given by TBT can be written as

$$\begin{aligned} u_x &= u_{x_1} \\ u_y &= u_{y_1} + x u_{y_2} + z u_{y_3} \\ u_z &= u_{z_1} \end{aligned} \tag{1}$$

where the parameters on the right-hand sides ($u_{x_1}, u_{y_1}, u_{z_1}, u_{y_2}, u_{y_3}$) are the displacements and the rotations on the reference axis. EBBT requires a further condition, which results in the penalization of the shear strain components ϵ_{xy} and ϵ_{zy}.

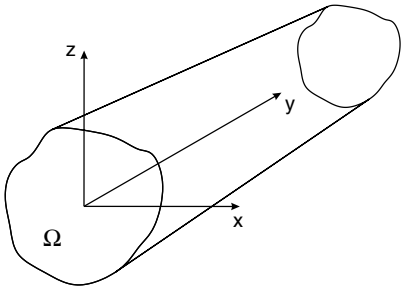

Fig. 1 Coordinate frame of the beam model.

If EBBT is applied to the idealized semimonocoque assumptions, it is possible to reduce redundancy in statically indeterminate structures. This method, hereafter referred to as the beam semimonocoque (BS) model, is certainly less accurate than PS because more assumptions are required. It should be noted that, for statically determinate structures, the two methods coincide.

C. Refined Beam Models Based on Taylor Expansion

Several higher-order beam models can be found in open literature to overcome planar conditions on the displacement field over the wing cross-section. The Taylor-based CUF can be adopted to refine the displacement field of classical 1-D models by adding expansion terms in Eq. (1). For instance, the TE second-order ($N = 2$) refined 1-D model presents the following kinematic model:

$$\begin{aligned} u_x &= u_{x_1} + xu_{x_2} + zu_{x_3} + x^2u_{x_4} + xzu_{x_5} + z^2u_{x_6} \\ u_y &= u_{y_1} + xu_{y_2} + zu_{y_3} + x^2u_{y_4} + xzu_{y_5} + z^2u_{y_6} \\ u_z &= u_{z_1} + xu_{z_2} + zu_{z_3} + x^2u_{z_4} + xzu_{z_5} + z^2u_{z_6} \end{aligned} \tag{2}$$

The 1-D model described by Eq. (2) has 18 generalized displacement variables: three constant, six linear, and nine parabolic terms. The possibility of refining 1-D models allows us to deal with a wide variety of problems with no need for ad hoc formulations. Nonclassical effects (e.g., warping, in-plane deformations, shear effects, bending-torsion couplings) are accounted for by opportunely varying the order of the adopted model. More details about TE models can be found in Sec. III and in the book by Carrera et al. [24].

D. Component-Wise

In a wing structural analysis, each component (e.g., ribs, stringers, panels, etc.) is commonly modeled through different elements (e.g., beams, shells, solids, etc.). For instance, by considering a simplified wing box (see Fig. 2), stringers are considered as beams, whereas panels and ribs are modeled with two-dimensional (2-D) plate elements. 3-D elasticity elements could also be used for stringers or for both stringers and panels. In the present paper, 1-D LE elements were used to simultaneously model all the wing components. In a finite element framework, this means that spar caps, webs, panels, and ribs are modeled by means of the same 1-D finite element and, therefore, with no need of ad hoc formulations for each component. More details about the LE beam theory and the implementation of CW models can be found in Sec. III.

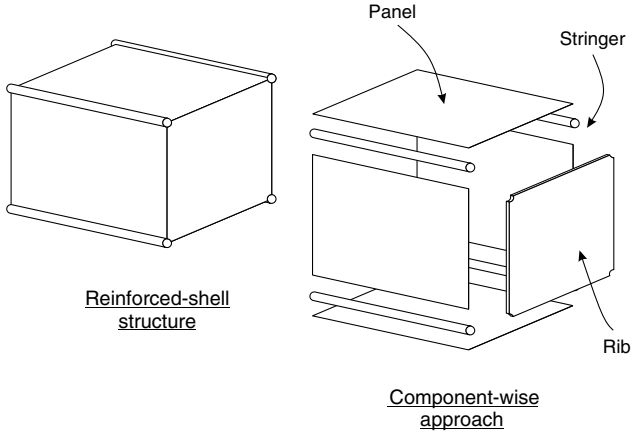

Fig. 2 Component-wise approach.

III. One-Dimensional Carrera Unified Formulation

In this section, a brief description of models based on CUF is provided. First, some notations are introduced. Then, TE and LE models are described. In Sec. III.C, the higher-order finite elements are formulated. Finally, in Sec. III.D, the use of the LE 1-D elements in CW models is discussed.

A. Preliminaries

Referring to the coordinate frame shown in Fig. 1, let us introduce the transposed displacement vector,

$$\mathbf{u}(x, y, z) = \{\, u_x \quad u_y \quad u_z \,\}^T \tag{3}$$

The cross-section of the structure is Ω, and the beam boundaries over y are $0 \le y \le L$. The stress and strain components ($\boldsymbol{\sigma}$ and ϵ, respectively) are grouped as follows:

$$\begin{aligned} \boldsymbol{\sigma}_p &= \{\, \sigma_{zz} \quad \sigma_{xx} \quad \sigma_{zx} \,\}^T, \\ \epsilon_p &= \{\, \epsilon_{zz} \quad \epsilon_{xx} \quad \epsilon_{zx} \,\}^T \\ \boldsymbol{\sigma}_n &= \{\, \sigma_{zy} \quad \sigma_{xy} \quad \sigma_{yy} \,\}^T, \\ \epsilon_n &= \{\, \epsilon_{zy} \quad \epsilon_{xy} \quad \epsilon_{yy} \,\}^T \end{aligned} \tag{4}$$

The subscript "n" stands for terms lying on the cross-section, while "p" stands for terms lying on planes that are orthogonal to Ω. In the case of small displacements with respect to a characteristic dimension of Ω, linear strain–displacement relations can be used:

$$\epsilon_p = \boldsymbol{D}_p\mathbf{u} \quad \epsilon_n = \boldsymbol{D}_n\mathbf{u} = (\boldsymbol{D}_{n\Omega} + \boldsymbol{D}_{ny})\mathbf{u} \tag{5}$$

where $\boldsymbol{D}_p$ and $\boldsymbol{D}_n$ are linear differential operators,

$$\boldsymbol{D}_p = \begin{bmatrix} 0 & 0 & \frac{\partial}{\partial z} \\ \frac{\partial}{\partial x} & 0 & 0 \\ \frac{\partial}{\partial z} & 0 & \frac{\partial}{\partial x} \end{bmatrix}, \quad \boldsymbol{D}_{n\Omega} = \begin{bmatrix} 0 & \frac{\partial}{\partial z} & 0 \\ 0 & \frac{\partial}{\partial x} & 0 \\ 0 & 0 & 0 \end{bmatrix}, \quad \boldsymbol{D}_{ny} = \begin{bmatrix} 0 & 0 & \frac{\partial}{\partial y} \\ \frac{\partial}{\partial y} & 0 & 0 \\ 0 & \frac{\partial}{\partial y} & 0 \end{bmatrix} \tag{6}$$

Constitutive laws were exploited to obtain stress components,

$$\boldsymbol{\sigma} = \boldsymbol{C}\boldsymbol{\epsilon} \tag{7}$$

According to Eq. (4), Eq. (7) becomes

$$\begin{aligned} \boldsymbol{\sigma}_p &= \tilde{\boldsymbol{C}}_{pp}\boldsymbol{\epsilon}_p + \tilde{\boldsymbol{C}}_{pn}\boldsymbol{\epsilon}_n \\ \boldsymbol{\sigma}_n &= \tilde{\boldsymbol{C}}_{np}\boldsymbol{\epsilon}_p + \tilde{\boldsymbol{C}}_{nn}\boldsymbol{\epsilon}_n \end{aligned} \tag{8}$$

In the case of isotropic material, the matrices $\tilde{\boldsymbol{C}}_{pp}, \tilde{\boldsymbol{C}}_{nn}, \tilde{\boldsymbol{C}}_{pn}$, and $\tilde{\boldsymbol{C}}_{np}$ are

$$\tilde{\boldsymbol{C}}_{pp} = \begin{bmatrix} \lambda + 2G & \lambda & 0 \\ \lambda & \lambda + 2G & 0 \\ 0 & 0 & G \end{bmatrix}, \quad \tilde{\boldsymbol{C}}_{nn} = \begin{bmatrix} G & 0 & 0 \\ 0 & G & 0 \\ 0 & 0 & \lambda + 2G \end{bmatrix},$$
$$\tilde{\boldsymbol{C}}_{pn} = \tilde{\boldsymbol{C}}_{np}^T = \begin{bmatrix} 0 & 0 & \lambda \\ 0 & 0 & \lambda \\ 0 & 0 & 0 \end{bmatrix} \tag{9}$$

where G and λ are the Lamé's parameters. If Poisson ν and Young E moduli are used, one has $G = \frac{E}{2(1+\nu)}$ and $\lambda = \frac{\nu E}{(1+\nu)(1-2\nu)}$. Additional details can be found in [35] and [36].

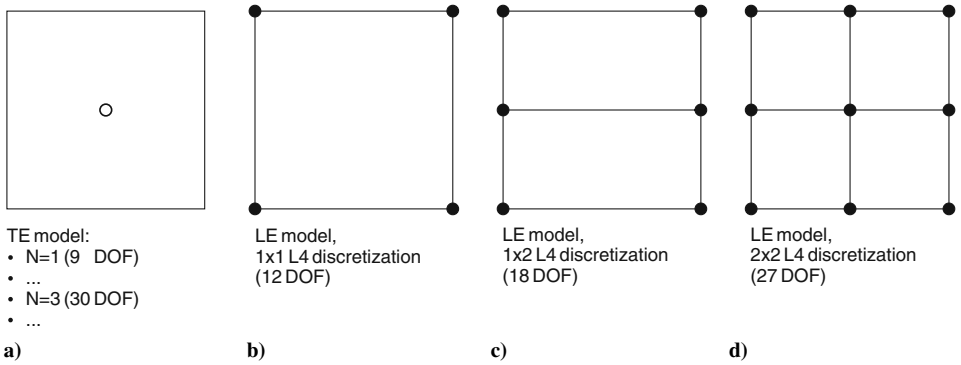

Fig. 3 Differences between the TE and LE models.

B. One-Dimensional Advanced Formulation with Variable (Hierarchial) Kinematics

In the framework of the CUF, the displacement field above the cross-section is the expansion of generic functions F_τ:

$$\mathbf{u}(x, y, z) = F_\tau(x, z)\mathbf{u}_\tau(y), \qquad \tau = 1, 2, \ldots, M \tag{10}$$

where F_τ vary over the cross-section, $\mathbf{u}_\tau$ is the displacement vector, and M stands for the number of terms of the expansion. According to the Einstein notation, the repeated subscript τ indicates summation. The choice of F_τ determines the class of 1-D CUF model that has to be adopted. Two cases are addressed in this paper: TE and LE.

1-D TE models are based on polynomial expansions, $x^i z^j$, of the displacement field above the cross-section of the structure, where i and j are positive integers. A generic N-order displacement field is therefore expressed by

$$\mathbf{u} = \sum_{N_i=0}^{N} \left(\sum_{M=0}^{N_i} x^{N-M} z^M \mathbf{u}_{\frac{N(N+1)+M+1}{2}} \right) \tag{11}$$

Equation (2) is a particular case of Eq. (11). The order N of the expansion is arbitrary and defines the beam theory. N is set as an input of the analysis. The choice of N, for a given structural problem, is usually made through a convergence study.

The refined TE models described previously are characterized by degrees of freedom (displacements and N-order derivatives of displacements) with a correspondence to the axis of the beam (see Fig. 3). The expansion can also be made by using only pure displacement values, e.g., by using Lagrange polynomials. The LE class exploits Lagrange-like polynomials to build 1-D higher-order models. In this work, two types of cross-section polynomial sets were adopted: four-point elements (L4) and nine-point elements (L9). The isoparametric formulation was exploited to deal with arbitrary shaped geometries. The L4 interpolation functions are given in [37]:

$$F_\tau = \frac{1}{4}(1 + rr_\tau)(1 + ss_\tau) \qquad \tau = 1, 2, 3, 4 \tag{12}$$

where r and s vary from -1 to $+1$, whereas r_τ and s_τ are the coordinates of the four points whose numbering and location in the natural coordinate frame are shown in Fig. 4a. In the case of an L9 element, the interpolation functions are given by

$$\begin{aligned} F_\tau &= \frac{1}{4}(r^2 + rr_\tau)(s^2 + ss_\tau) \quad \tau = 1, 3, 5, 7 \\ F_\tau &= \frac{1}{2}s_\tau^2(s^2 + ss_\tau)(1 - r^2) + \frac{1}{2}r_\tau^2(r^2 + rr_\tau)(1 - s^2) \quad \tau = 2, 4, 6, 8 \\ F_\tau &= (1 - r^2)(1 - s^2) \quad \tau = 9 \end{aligned} \tag{13}$$

The nine points of the L9 element are shown in Fig. 4b. For instance, the displacement field given by an L4 element is

$$\begin{aligned} u_x &= F_1 u_{x_1} + F_2 u_{x_2} + F_3 u_{x_3} + F_4 u_{x_4} \\ u_y &= F_1 u_{y_1} + F_2 u_{y_2} + F_3 u_{y_3} + F_4 u_{y_4} \\ u_z &= F_1 u_{z_1} + F_2 u_{z_2} + F_3 u_{z_3} + F_4 u_{z_4} \end{aligned} \tag{14}$$

where $u_{x_1}, \ldots, u_{z_4}$ are the displacement variables of the problem and represent the translational displacement components of each of the four points of the L4 element. The adopted cross-section displacement field (L4 or L9) defines the beam theory. For further refinements, the cross-section can be discretized by using several L-elements as in Figs. 3b–3d. More details about LE models can be found in the paper by Carrera and Petrolo [30].

C. Finite Element Formulation Based on Lagrange Expansion and Taylor Expansion

The FE approach was adopted to discretize the structure along the y-axis. This process is conducted via a classical finite element technique, where the displacement vector is given by

$$\mathbf{u}(x, y, z) = F_\tau(x, z)N_i(y)\mathbf{q}_{\tau i} \tag{15}$$

where N_i stands for the shape functions, and $\mathbf{q}_{\tau i}$ is the nodal displacement vector:

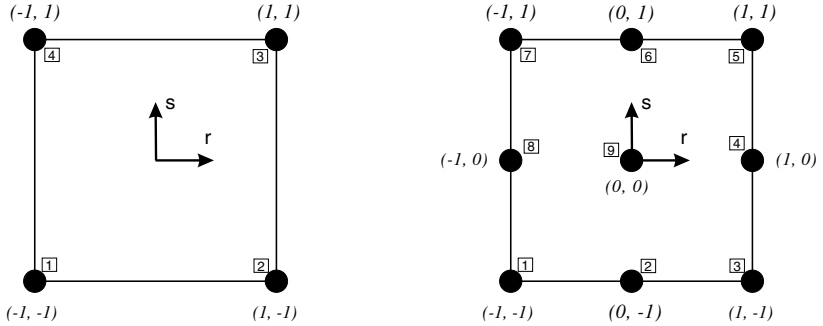

a) Four-point element, L4 **b) Nine-point element, L9**

Fig. 4 Cross-section L elements in natural geometry.

$$\mathbf{q}_{\tau i} = \{\, q_{u_{x_{\tau i}}} \quad q_{u_{y_{\tau i}}} \quad q_{u_{z_{\tau i}}} \,\}^T \tag{16}$$

For the sake of brevity, the shape functions are not reported here. They can be found in many books, for instance in [38]. Elements with four nodes (B4) were adopted in this work, that is, a cubic approximation along the y-axis was assumed. The choice of the cross-section discretization for the LE class (i.e., the choice of the type, the number and the distribution of cross-section elements) or the theory order N for the TE class is completely independent of the choice of the beam finite element to be used along the axis of the beam.

The stiffness matrix of the elements and the external loadings vector were obtained via the PVD:

$$\delta L_{\text{int}} = \int_V (\delta \epsilon_p^T \boldsymbol{\sigma}_p + \delta \epsilon_n^T \boldsymbol{\sigma}_n)\, \mathrm{d}V = \delta L_{\text{ext}} \tag{17}$$

where L_{int} stands for the strain energy, L_{ext} is the work of the external loadings, and δ stands for the virtual variation. The virtual variation of the strain energy was rewritten using Eqs. (5), (8), (10), and (15):

$$\delta L_{\text{int}} = \delta \mathbf{q}_{\tau i}^T \mathbf{K}^{ij\tau s} \mathbf{q}_{sj} \tag{18}$$

where $\mathbf{K}^{ij\tau s}$ is the stiffness matrix in the form of the fundamental nucleus. In a compact notation, it can be written as

$$\begin{aligned}
\boldsymbol{K}^{ij\tau s} = {} & I_l^{ij} \lhd (\boldsymbol{D}_{np}^T F_\tau \boldsymbol{I})[\tilde{\boldsymbol{C}}_{np}(\boldsymbol{D}_p F_s \boldsymbol{I}) + \tilde{\boldsymbol{C}}_{nn}(\boldsymbol{D}_{np}(\boldsymbol{D}_{np} F_s \boldsymbol{I})] \\
& + (\boldsymbol{D}_p^T F_\tau \boldsymbol{I})[\tilde{\boldsymbol{C}}_{pp}(\boldsymbol{D}_p F_s \boldsymbol{I}) + \tilde{\boldsymbol{C}}_{pn}(\boldsymbol{D}_{np} F_s \boldsymbol{I})] \rhd_\Omega \\
& + I_l^{ij_y} \lhd [(\boldsymbol{D}_{np}^T F_\tau \boldsymbol{I})[\tilde{\boldsymbol{C}}_{nn} + (\boldsymbol{D}_p^T F_\tau \boldsymbol{I})\tilde{\boldsymbol{C}}_{pn}] F_s \rhd_\Omega \boldsymbol{I}_{\Omega y} \\
& + I_l^{i_y j} \boldsymbol{I}_{\Omega y} \lhd F_\tau [\tilde{\boldsymbol{C}}_{np}(\boldsymbol{D}_p F_s \boldsymbol{I}) + \tilde{\boldsymbol{C}}_{nn}(\boldsymbol{D}_{np} F_s \boldsymbol{I})] \rhd_\Omega \\
& + I_l^{i_y j_y} \boldsymbol{I}_{\Omega y} \lhd F_\tau \tilde{\boldsymbol{C}}_{nn} F_s \rhd_\Omega \boldsymbol{I}_{\Omega y}
\end{aligned} \tag{19}$$

where

$$\boldsymbol{I}_{\Omega y} = \begin{bmatrix} 0 & 1 & 0 \\ 1 & 0 & 0 \\ 0 & 0 & 1 \end{bmatrix} \lhd \ldots \rhd_\Omega = \int_\Omega \ldots \, \mathrm{d}\Omega \tag{20}$$

$$(I_l^{ij}, I_l^{ij_y}, I_l^{i_y j}, I_l^{i_y j_y}) = \int_l (N_i N_j, N_i N_{j_y}, N_{i_y} N_j, N_{i_y} N_{j_y})\, \mathrm{d}y \tag{21}$$

It should be noted that $\mathbf{K}^{ij\tau s}$ does not depend either on the expansion order or on the choice of the F_τ expansion polynomials. These are the key points of CUF, which allows, with only nine FORTRAN statements, the implementation of any order of multiple class theories.

The loadings vector, which is variationally coherent to the model, was derived for the case of a generic concentrated load $\mathbf{P}$ acting on the application point (x_p, y_p, z_p):

$$\mathbf{P} = \{\, P_{u_x} \quad P_{u_y} \quad P_{u_z} \,\}^T \tag{22}$$

Any other loading condition can be similarly treated. The virtual work due to $\mathbf{P}$ is

$$\delta L_{\text{ext}} = \mathbf{P} \delta \mathbf{u}^T \tag{23}$$

According to Eq. (10), one has

$$\delta L_{\text{ext}} = F_\tau \mathbf{P} \delta \mathbf{u}_\tau^T \tag{24}$$

By introducing the nodal displacements and the shape functions, Eq. (24) becomes

$$\delta L_{\text{ext}} = F_\tau N_i \mathbf{P} \delta \mathbf{q}_{\tau i}^T \tag{25}$$

where F_τ and N_i are evaluated in (x_p, z_p) and y_p, respectively. The last equation allows for the identification of the components of the nucleus that have to be loaded, that is, it allows for the proper assembling of the loading vector by detecting the displacement variables that have to be loaded.

A detailed description of 1-D formulations based on CUF can be found in the recent book by Carrera et al. [24].

D. Component-Wise Models Through One-Dimensional Lagrange Expansion Elements

The LE formulation was used in this paper to implement CW models of reinforced-shell wing structures, as shown in Fig. 5a, where a two-stringer spar is considered. Figure 5b shows a possible CW model of the spar where each component was modeled via one 1-D LE element. Each LE element is then assembled above the cross-section to obtain the global stiffness matrix based on the 1-D formulation. Because panels could not be reasonably modeled via a 1-D formulation, 1-D CW models can be refined by using several L elements for one component. This aspect is shown in Fig. 5c, where the panel is modeled via two 1-D LE elements. By exploiting the present 1-D formulation, the analysis capabilities of a structural model can be enhanced by 1) locally refining the LE discretization, or 2) using higher-order LE elements (e.g., 4-node, 9-node, 16-node).

IV. Numerical Results

The various approaches considered to wing structure analysis are evaluated in this section and compared to commercial FEM software results.

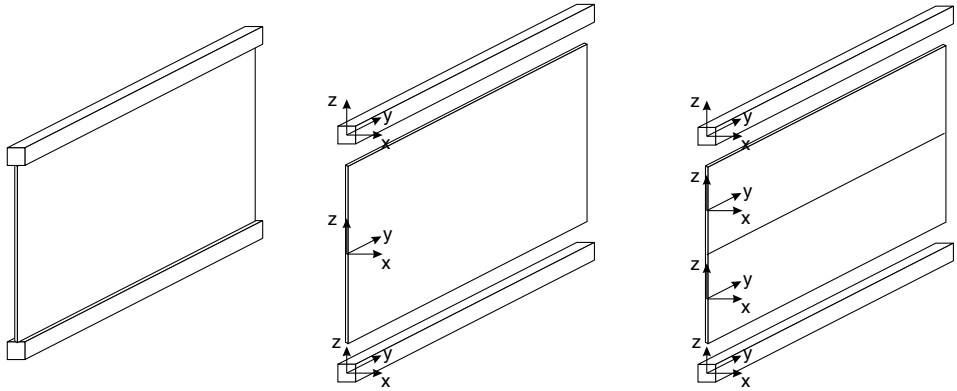

a) Two-stringer spar **b) Each of the two stringers and the panel are modelled with one LE 1D element** **c) This panel is modelled with two 1D LE elements**

Fig. 5 CW approach through LE elements.

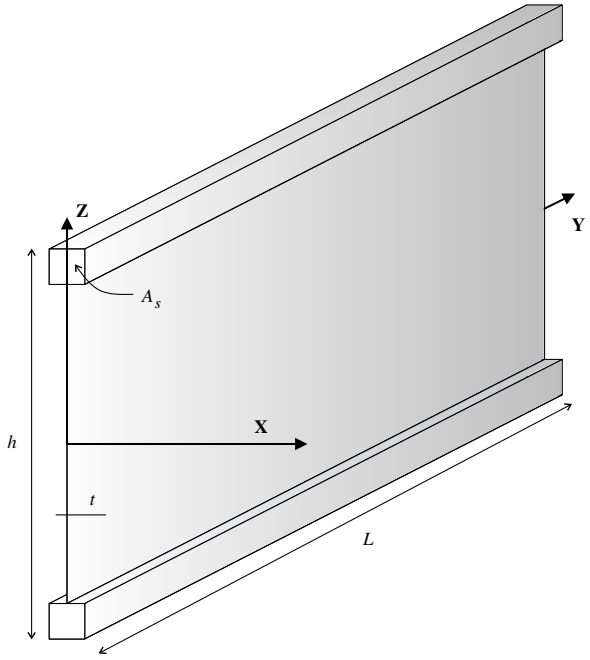

Fig. 6 Two-stringer spar.

Two classical spars are considered for the first assessment. Then, two more complex wing structures are analyzed to show the capability of the present CUF models of dealing with ribs and open sections. Unless otherwise stated, the results by refined and CW models are compared to 3-D solid FEM models because the present models are not affected by the discontinuities in the displacement fields that may result from a combination of 1-D, 2-D, and 3-D elements. TE and LE models are also compared with classical beam theories and analytical results by theories based on idealized stiffened-shell structures for further comparisons. Particular attention is given to the capabilities offered by CW models of dealing with thin-walled reinforced structures as well as with solid and shell-like FEM analyses with significantly lower computational costs.

A. Two-Stringer Spar

The simplest spar structure shown in Fig. 6 was considered first. Stringers were taken to be rectangular for convenience; however, their shape does not affect the validity of the proposed analysis. The geometrical data are as follows: axial length $L = 3$ m, cross-section height, $h = 1$ m, area of the spar caps $A_s = 0.9 \times 10^{-3}$ m^2, web thickness $t = 1 \times 10^{-3}$ m. The whole structure is made of an aluminum alloy material. The material data are as follows: Young's modulus $E = 75$ GPa, Poisson ratio $\nu = 0.33$. The beam was clamped at $y = 0$ and a point load $F_z = -1 \times 10^4$ N was applied at $[0, L, 0]$.

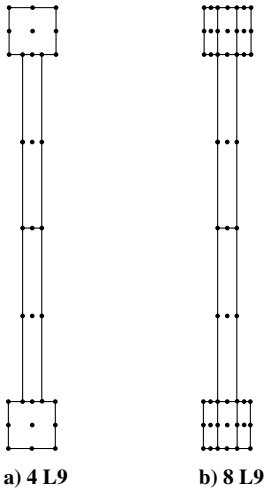

a) 4 L9 **b) 8 L9**

Fig. 7 Cross-section L9 distributions for the LE models of the two-stringer spar.

The vertical displacement u_z at the loaded point is reported in Table 1. Results were related to an MSC/NASTRAN FE model with eight-node solid elements and to classical beam theories EBBT and TBT. Refined theories related to higher-order TE models are also reported in Table 1. N refers to the expansion order of the TE beam theory. Component-wise LE results are given. These models were obtained by using two different L9 cross-section distributions, as shown in Fig. 7. All of the 1-D CUF models were implemented by considering 10 B4 elements along the y-axis because this mesh offers good accuracy. A detailed analysis of the effects of the number and the type of finite elements along the beam axis can be found in [24]. The third column in Table 1 quotes the number of DOFs for each model. DOFs are used to estimate the computational efficiency of the proposed models. In fact, it should be noticed that another advantage given by 1-D formulations is that they can, in general, lead to lower stiffness-matrix bandwidths with respect to 2-D or 3-D FE mathematical models.

It should be noted that the CW FE approach uses only physical surfaces (the four faces of caps as well as the inner and outer surfaces of the panel) to build FE mathematical models. The FE models and the classical beam and plate/shell approaches usually introduce artificial surfaces and lines (e.g., the beam axis and the reference surface for shell elements). This characteristic of CW models is a unique feature that makes this approach advantageous in a computer-aided engineering/computer-aided design (CAE/CAD) scenario.

Table 1 Displacement values u_z at the loaded point, two-stringer spar

	$u_z \times 10^3$, m	DOFs
	Analytical methods	
BS	−2.671	—
PS	−3.059	—
	Classical beam theories	
EBBT	−1.827	279
TBT	−2.117	279
	TE	
$N = 3$	−2.514	930
$N = 5$	−2.629	1953
$N = 7$	−2.738	3348
$N = 9$	−2.890	5115
	CW	
4 L9 (Fig. 7a)	−3.639	2883
8 L9 (Fig. 7b)	−3.639	4743
	MSC/NASTRAN	
Solid	−3.815	76,050

Table 2 Axial load in the upper stringer, P, at $y = 0$ and mean shear flow on the sheet panel, q, at $y = \frac{L}{2}$, two-stringer spar

	P, N[a]	q, N/m[a]
	Analytical methods	
BS	3.192	−1.064
PS	3.192	−1.064
	Classical beam theories	
EBBT	1.993	−0.274
TBT	1.993	−0.274
	TE	
$N = 3$	2.434	
$N = 5$	2.350	−0.561
	CW	
4 L9 (Fig. 7a)	2.833	−1.034
8 L9 (Fig. 7b)	2.739	−1.035
	MSC/NASTRAN	
Solid	2.713	−1.036

[a]All values are multiplied $\times 10^{-4}$.

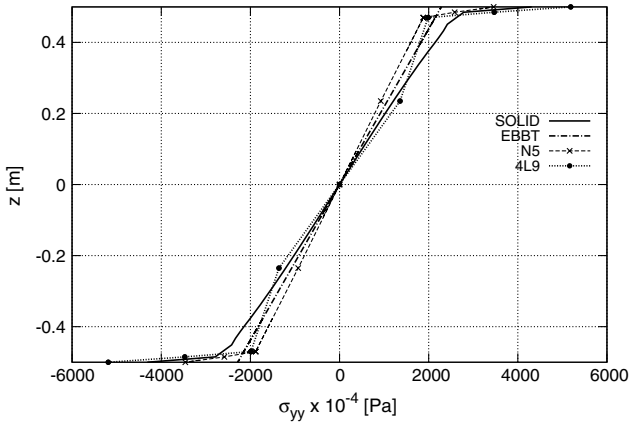

a) σ_{yy} vs z at $x = y = 0$

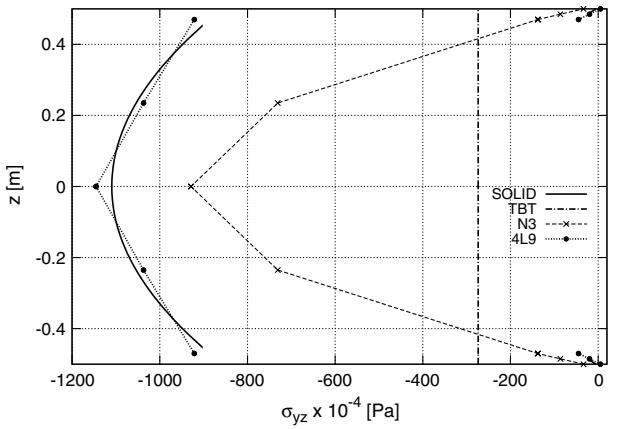

b) σ_{yz} vs z at $x = 0$, $y = \frac{L}{2}$

Fig. 8 Axial stress σ_{yy} and shear stress σ_{yz} vs the z-axis, two-stringer spar.

The analytical results related to the BS and PS approaches are provided and evaluated as follows (see [3]):

$$u_{z_{BS}} = \frac{F_z L^3}{3EI}, \qquad u_{z_{PS}} = \frac{F_z L^3}{3EI} + \frac{F_z L}{AG} \tag{26}$$

where I is the cross-section moment of inertia about the x-axis, G is the shear modulus, and A is the overall cross-section area. In the present paper, stress fields are evaluated in terms of axial loads in stringers and shear flows on panels/webs, to compare the results with classical analytical models. Table 2 reports the axial load in the upper stringer, P, at $y = 0$ and the mean shear flow in the panel, q, at $y = \frac{L}{2}$. In accordance with [3], for both BS and PS analytical models, P and q were evaluated as

$$P = \frac{F_z L}{\bar{h}}, \qquad q = -\frac{F_z}{\bar{h}} \tag{27}$$

where $\bar{h}$ is the distance between the centers of the two stringers.

CUF and solid models are not affected by the generalization of the classical ideal reinforced-shell assumptions. For this reason, the shear flows acting on panels in 1-D refined CUF models and in MSC/NASTRAN are not constant within the panels and are reported as mean shear flows, evaluated as

Table 3 Displacement values u_z at the loaded point and axial load in the upper stringer, P, at $y = 0$, two-stringer spar

	$u_z \times 10^3$, m	P, N	DOFs
Solid 1	−3.785	2.577	2805
Solid 2	−3.815	2.713	76,050
Solid 3	−3.862	2.709	198,246

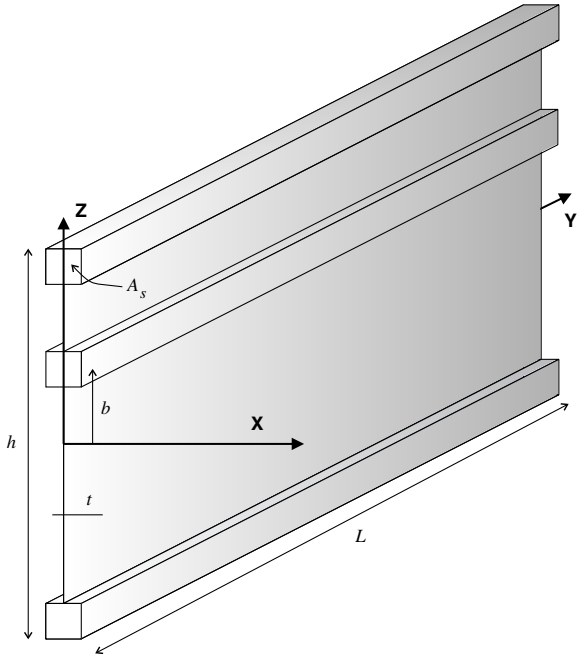

Fig. 9 Three-stringer spar.

Table 4 Displacement values u_z at the center of the intermediate stringer, three-stringer spar

	$u_z \times 10^3$, m	DOFs
	Analytical methods	
BS	−1.309	—
PS	−1.471	—
	Classical beam theories	
EBBT	−1.325	279
TBT	−1.487	279
	TE	
$N = 4$	−1.661	1395
$N = 6$	−1.707	2604
$N = 8$	−1.730	4185
	CW	
5 L9	−1.846	3813
	MSC/NASTRAN	
Solid	−1.857	72,450

Table 5 Axial loads in the stringers at $y = 0$ and mean shear flows on the sheet panels at $y = \frac{L}{2}$, three-stringer spar

	q_1, N/m[a]	q_2, N/m[a]	P_1, N[a]	P_2, N[a]	P_3, N[a]
		Analytical methods			
BS	−0.859	−1.095	2.574	0.730	−3.285
PS	−0.949	−1.118	2.847	0.507	−3.353
		Classical beam theory			
EBBT	−0.305	−0.305	2.323	0.733	−2.766
TBT	−0.305	−0.305	2.323	0.733	−2.766
		TE			
$N = 4$	−0.071	−0.902	3.208	0.081	−3.202
$N = 6$	−0.402	−1.006	2.997	0.727	−3.251
$N = 8$	−0.469	−1.052	2.916	0.639	−3.215
		CW			
5 L9	−0.820	−1.150	2.495	0.633	−2.980
		MSC/NASTRAN			
Solid	−0.816	−1.150	2.457	0.572	−2.781

[a]All values are multiplied $\times 10^{-4}$.

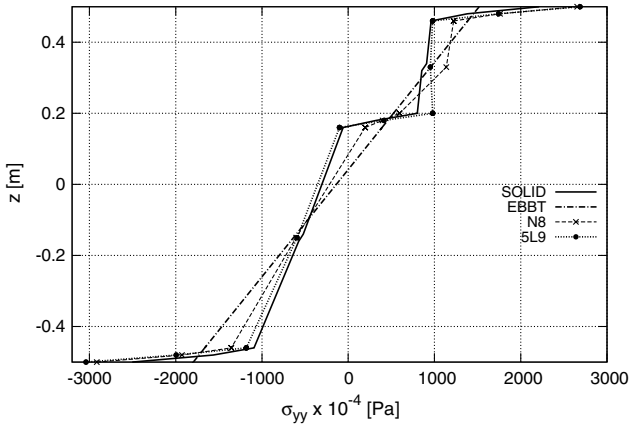

a) σ_{yy} vs z at $x = y = 0$

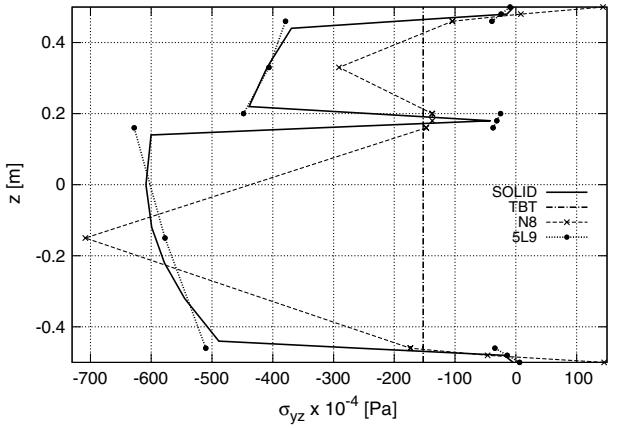

b) σ_{yz} vs z at $x = 0$, $y = \frac{L}{2}$

Fig. 10 Axial stress σ_{yy} and shear stress σ_{yz} vs the z-axis, three-stringer spar.

$$q_m = \frac{1}{l}\int_A \tau \, \mathrm{d}A$$

Conversely, in both MSC/NASTRAN and CUF models, P was computed by evaluating the constraint forces multiplying the non-constrained stiffness matrix by the displacement vector.

The variation in the axial stress and the shear stress versus the z-axis is presented in Fig. 8. Results by solid, TE, LE, and classical beam models are reported. A convergence study was carried out for MSC/NASTRAN models, and the results are shown in Table 3. The following considerations arise from the analyses.

1) Refined beam theories, especially LE, allow us to obtain the results of the solid model (which is the most accurate and at the same time the most computationally expensive).

2) The number of degrees of freedom of the present models is significantly reduced with respect to the MSC/NASTRAN solid model.

3) Both MSC/NASTRAN and higher-order CUF models, unlike analytical theories based on idealized stiffened-shell structures and classical 1-D models, highlight the fact that the axial stress component σ_{yy} is not linear versus z and that the shear stress component σ_{yz} is not constant along the sheet panel.

4) The component-wise capability of the present LE approach is clearly evident from the conducted analysis.

B. Three-Stringer Spar

A longeron with three longitudinal stiffeners was subsequently considered. The geometry of the structure is shown in Fig. 9. The spar was clamped at $y = 0$, whereas a point load F_z was applied at the center of the upper stringer at $y = L$. The magnitude of F_z is equal to -1×10^4 N. The geometrical characteristics were as follows: axial length $L = 3$ m, cross-section height $h = 1$ m, area of the stringers $A_s = 1.6 \times 10^{-3}$ m^2, sheet panel thickness $t = 2 \times 10^{-3}$ m, distance from the intermediate stringer to the x–y plane, $b = 0.18$ m. The whole structure is made of the same isotropic material as in the previous case.

Table 4 shows the displacement u_z evaluated at the center of the intermediate stringer together with the indication of the number of degrees of freedom for each considered model. In the first and second rows, classical analytical models results are reported. The increasing-order Taylor-type models are considered in rows 3 to 7. The CW LE model was obtained by discretizing the cross-section with 5 L9 elements, one for each spar component (stringers and webs), and the results are shown in row 7. The last row shows the solid model result obtained by an FE model in MSC/NASTRAN. The solid model was obtained so as to guarantee a low aspect ratio of the 8-node solid elements.

Table 5 shows the stress fields of the considered structure. Axial loads in the top (P_1), middle (P_2), and bottom (P_3) stringers are evaluated at $y = 0$, together with the mean shear flows on the upper (q_1) and bottom (q_2) sheet panels at $y = \frac{L}{2}$. Referring to the BS model, the axial loads in the stringers were evaluated by means of the Navier equation that gives the longitudinal normal stress distribution over the spar section. Considering a coordinate frame laying on the center of mass, the following equation holds:

$$P_{i_{BS}} = \frac{F_z L}{I} A_i Z_i \tag{28}$$

where P_i is the axial force in the ith stringer, A_i is the concentrated boom area, and Z_i is the vertical coordinate. The shear flows q_i were evaluated from the equilibrium equations. For the structural configuration analyzed, the PS differs from the BS solution. In fact, the three-stringer spar has one redundance (q_1 and q_2 consist of two independent unknowns along the z-axis, which are related by only one common equilibrium equation). The PVD was employed to take

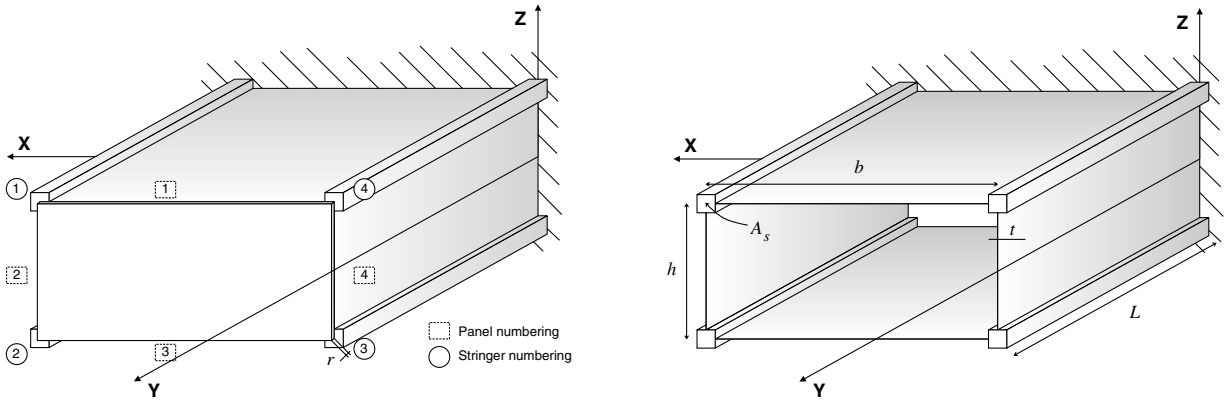

a) **b)**

Fig. 11 Rectangular wing boxes.

Table 6 Convergence of the CW models; mean shear flows in the sheet panels at the $y = L/2$ and axial loads in the stringers at $y = 0$ for the rectangular wing box

	q_1, N/m[a]	q_2, N/m[a]	q_3, N/m[a]	q_4, N/m[a]	P_1, N[a]	P_2, N[a]	P_3, N[a]	P_4, N[a]	DOFs
				CW					
8 L9	5.092	−5.173	−5.121	−16.624	23.313	−23.313	−26.211	26.211	6588
8 L9	(−0.032)[b]	(0.005)	(0.033)	(−21.789)	(−5.839)	(5.839)	(−55.007)	(55.007)	(5952)
12 L9	4.969	−5.171	−4.966	−16.654	21.033	−21.033	−24.603	24.603	9036
12 L9	(−0.164)	(0.013)	(0.164)	(−21.841)	(−5.488)	(5.488)	(−51.143)	(51.143)	(8184)
20 L9	5.037	−5.145	−5.034	−16.654	20.286	−20.286	−23.767	23.767	13,932
20 L9	(−0.061)	(0.010)	(0.092)	(−21.827)	(−5.235)	(5.235)	(−49.548)	(49.548)	(12,648)
				MSC/NASTRAN					
Solid/shell	5.077	−5.200	−5.149	−16.651	21.670	−21.670	−24.660	24.660	22,346
Solid/shell	(−0.381)	(0.293)	(−0.242)	(−21.530)	(−5.435)	(5.435)	(−51.765)	(51.765)	(22,020)
Solid	5.074	−5.104	−5.074	−16.368	20.166	−20.166	−22.942	22.942	115,362
Solid	(−0.071)	(0.011)	(0.071)	(−21.483)	(−5.163)	(5.163)	(−48.271)	(48.271)	(112,200)

[a]All values are multiplied $\times 10^{-3}$.
[b]Results by models without the rib are reported in brackets.

into account the deformability of stringers and panels. Let X be the redundant force in the lower longitudinal. By using the formula in [3], one has

$$X = \frac{\frac{E}{G}\left(\frac{h_2}{h_1}\right)\frac{1}{t} + \frac{2}{3}L^2\left(\frac{h_2}{h_1^2} + \frac{1}{2h_1}\right)\frac{1}{A}}{\frac{E}{G}\left(\frac{h_2^2}{h_1^2} + \frac{h_2}{L}\right)\frac{1}{t} + \frac{2}{3}L\left(\frac{h_2^2}{h_1^2} + \frac{h_2}{h_1} + 1\right)\frac{1}{A}} F_z \tag{29}$$

where h_1 is the distance between the top and the intermediate stringer, and h_2 is the distance between the intermediate and the bottom stringer. The axial forces $P_{i_{PS}}$ and the shear flows $q_{i_{PS}}$ were computed by substituting Eq. (29) in the equilibrium equations (for details, see [3]):

$$\begin{aligned}
P_{1_{PS}} &= -F_z\frac{L}{h_1} + X\frac{h_2}{h_1} \\
P_{2_{PS}} &= F_z\frac{L}{h_1} - X\left(1 + \frac{h_2}{h_1}\right) \\
P_{3_{PS}} &= X \\
q_{1_{PS}} &= \frac{F_z}{h_1} - X\frac{h_2}{Lh_1} \\
q_{2_{PS}} &= X\frac{1}{L}
\end{aligned} \tag{30}$$

The distribution of the axial stress σ_{yy} and the shear stress σ_{yz} versus the z-axis are shown in Fig. 10. The following statements hold.

1) The 5 L9 model is very close to the solid solution with a significant reduction of computational costs.

2) Results from Taylor-type models are less accurate than those from CW models.

3) The classical models are totally inadequate for the detection of stress fields of the considered structural problems.

4) Even in this particular case, the CW capability of the CUF-based LE approach is highly evident. Hence, the stress fields in the stringers/panels are described as accurately as those in the FE solids cases.

C. Rectangular Wing Box

A proper wing box both with and without a rib at the tip section (Fig. 11) was further analyzed. The length-to-width ratio L/b is equal to 3.125, with L as high as 3 m. The cross-section height h is equal to 0.46 m, whereas the thickness of the four sheet panels is $t = 2 \times 10^{-3}$ m. The area of the spar caps is $A_s = 1.6 \times 10^{-3}$ m^2. The wing box configuration with a rib at the tip presents a transversal stiffener with a thickness of $r = t$. The structure is made of the same isotropic material as in the previous cases. A point load $F_z = -1 \times 10^4$ N was applied at $[b, L, \frac{h}{2}]$.

First, a convergence study of the LE CW models was carried out. Table 6 shows the mean shear flows on the panels, the axial forces in

Table 7 Mean shear flows in the sheet panels at the $y = L/2$ and axial loads in the stringers at $y = 0$ for the rectangular wing box

	q_1, N/m[a]	q_2, N/m[a]	q_3, N/m[a]	q_4, N/m[a]	P_1, N[a]	P_2, N[a]	P_3, N[a]	P_4, N[a]	DOFs
				Analytical methods					
BS	5.435	−5.435	−5.435	−16.304	32.609	−32.609	−32.609	32.609	—
PS	5.221	−5.221	−5.221	−16.518	31.325	−31.325	−33.893	33.893	—
				Classical beam theories					
EBBT	0	−1.701	0	−1.701	19.757	−19.757	−19.757	19.757	306
TBT	0	−1.701	0	−1.701	19.757	−19.757	−19.757	19.757	306
				TE					
$N = 4$	4.470	−4.603	−4.470	−14.142	23.197	−23.197	−26.418	26.418	1530
$N = 4$	(4.769)[b]	(−4.897)	(−4.769)	(−13.848)	(23.167)	(−23.167)	(−26.448)	(26.448)	(1395)
$N = 6$	4.848	−4.579	−4.846	−14.218	23.529	−23.523	−27.567	27.556	2856
$N = 6$	(5.654)	(−5.329)	(−5.655)	(−13.467)	(23.404)	(−23.404)	(−27.684)	(27.686)	(2604)
$N = 8$	4.647	−5.148	−4.894	−16.240	23.803	−23.837	−26.579	26.722	4490
$N = 8$	(1.478)	(−1.204)	(−1.478)	(−20.060)	(1.555)	(−1.531)	(−48.968)	(48.976)	(4185)
				CW					
20 L9	5.037	−5.145	−5.034	−16.654	20.286	−20.286	−23.767	23.767	13,932
20 L9	(−0.061)	(0.010)	(0.092)	(−21.827)	(−5.235)	(5.235)	(−49.548)	(49.548)	(12,648)
				MSC/NASTRAN					
Solid/shell	5.077	−5.200	−5.149	−16.651	21.670	−21.670	−24.660	24.660	22,346
Solid/shell	(−0.381)	(0.293)	(−0.242)	(−21.530)	(−5.435)	(5.435)	(−51.765)	(51.765)	(22,020)
Solid	5.074	−5.104	−5.074	−16.368	20.166	−20.166	−22.942	22.942	115,362
Solid	(−0.071)	(0.011)	(0.071)	(−21.483)	(−5.163)	(5.163)	(−48.271)	(48.271)	(112,200)

[a]All values are multiplied $\times 10^{-3}$.
[b]Results by models without the rib are reported in brackets.

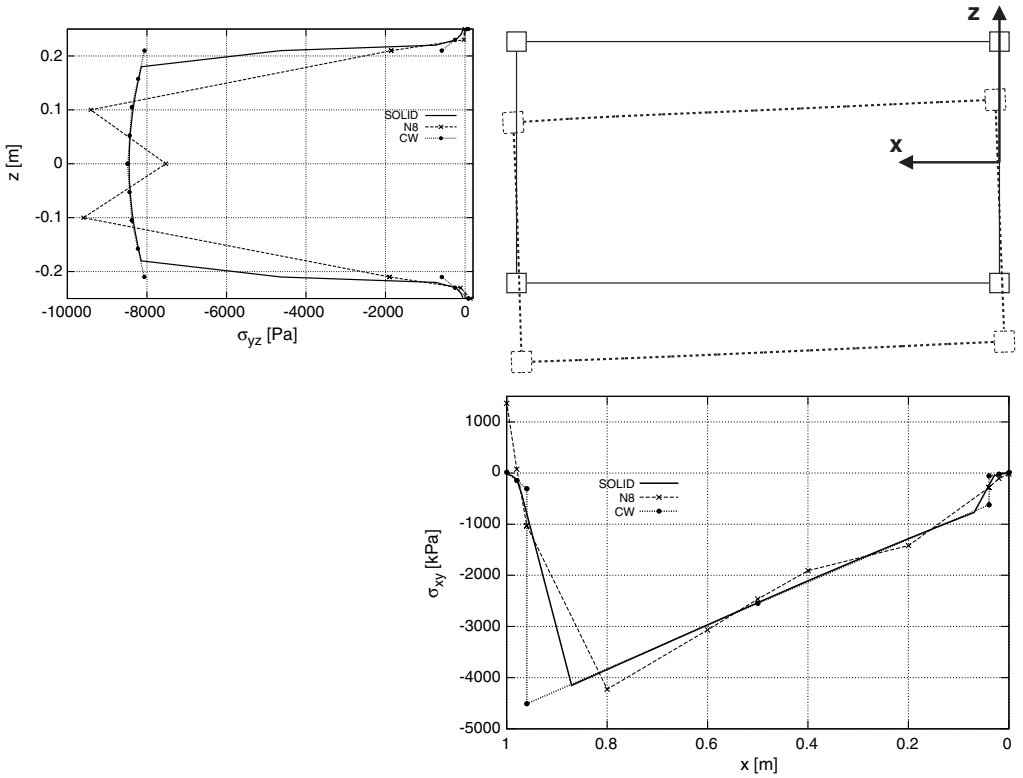

Fig. 12 σ_{yz} **vs the** z**-axis at** $x = b$**,** $y = \frac{L}{2}$ **and** σ_{xy} **versus the** x**-axis at** $z = -\frac{h}{2}$**,** $y = L/2$ **for the rectangular wing box with rib at the tip.**

the stringers, and the number of degrees of freedom for both CW and MSC/NASTRAN models of the rectangular wing box with the rib at the tip. In Table 6, results by the models of the rectangular wing box without the rib at the tip are shown in brackets. Each CW model has a different number of LE elements on the panels. In particular, in the 8 L9 model, stringers and panels were modeled with 1 L9 element each. In the 12 L9 model, one L9 element was used for each stringer and two elements were used for each panel. In the 20 L9 model, one L9 element was used for each stringer and four elements were used for each panel. The rib was discretized with a combination of L4 and L9 elements. The solid model was completely built with eight-node or 8-node solid elements, where as the solid/shell model was obtained as a combination of both solid and four-node or 4-node plate finite elements. Both stringers and the rib were discretized by means of solid elements in the solid/shell model, whereas plate elements were used for skins and webs. q_1 and P_1 refer to the top panel and to the top right stringer, respectively; q_2, q_3, q_4 and P_2, P_3, P_4 follow a clockwise enumeration as shown in Fig. 11. It should be underlined that LE

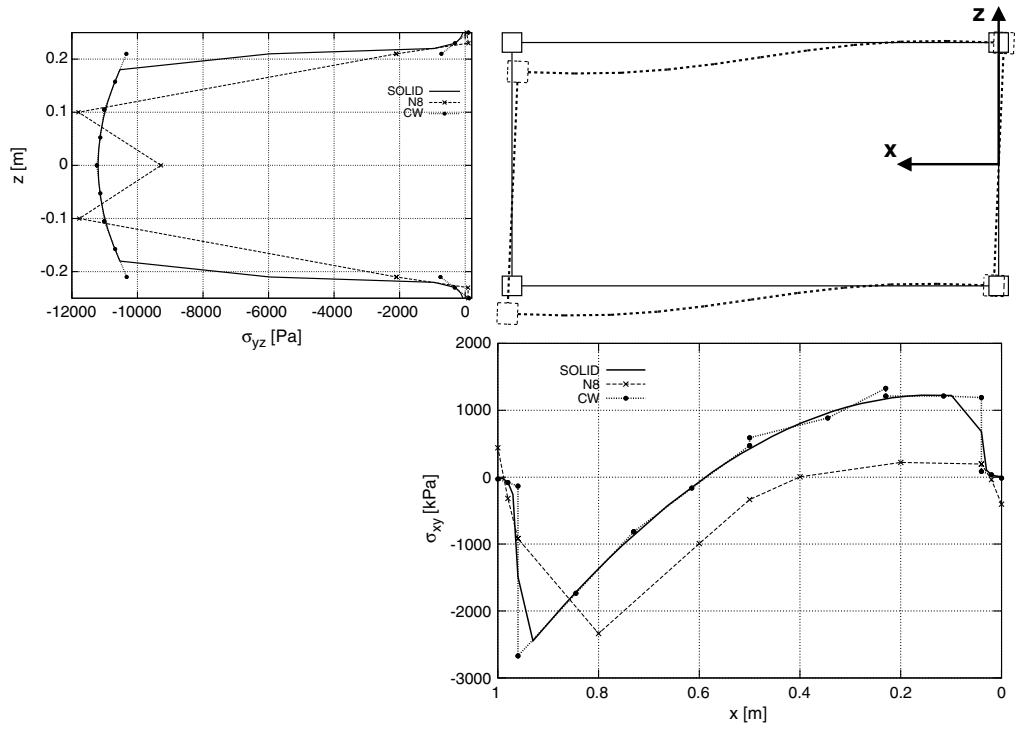

Fig. 13 σ_{yz} **vs the** z**-axis at** $x = b$**,** $y = L/2$ **and** σ_{xy} **vs the** x**-axis at** $z = -\frac{h}{2}$**,** $y = L/2$ **for the rectangular wing box with no rib.**

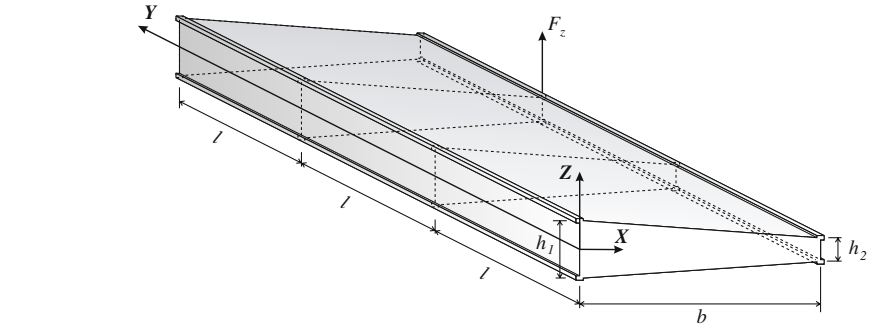

a) Full model

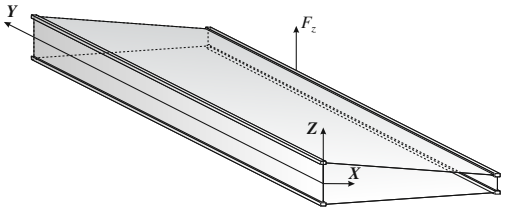

b) No ribs case

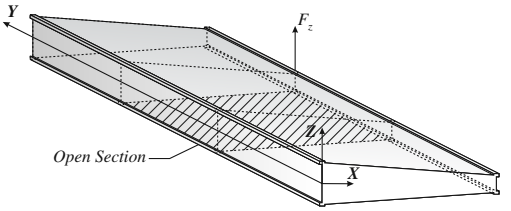

c) Full model with open mid-bay

Fig. 14 Different structural configurations of the three-bay wing box.

CW models, differently from TE, allow the local refinement of the components. For the structure considered, one L9 element was not sufficient to accurately detect the shear lag within the panel. Consequently, the axial forces in the stringers were not correct. The solution was enhanced by increasing the number of 1-D L9 elements used to discretize the panel.

Table 7 quotes the mean shear flows on the panels, the axial forces in the stringers, and the number of degrees of freedom for each implemented model of the rectangular wing box with the rib at the tip. Results from both analytical methods and classical beam theories are reported. Rows 5 to 7 consider the TE models. Finally, the convergent solution by the CW method is given in row 8, and the MSC/NASTRAN models are reported in the last two rows. In Table 7, the results for the rectangular wing box without the rib at the tip are shown in brackets.

BS and PS models (but also classical beam theories) are not able to correctly detect the behavior of the no-rib configuration of the rectangular wing box. In fact, one of the main assumptions of these methods is that the ribs are "rigid within their planes". The solutions provided by these methods for the wing box are described in the following. In accordance with the BS method, the axial forces and the shear flows were evaluated by solving first Eq. (28) and then the equilibrium equations. Conversely, as in the previous case, the PS solution requires the application of the PVD. Let X be the redundant force applied in the bottom left stringer [3]:

$$X = \frac{\frac{(b-h)}{4Gth}}{-\frac{4L}{3EA} - \frac{(b+h)}{2LGt}} F_z \tag{31}$$

Subsequently, PS stress fields were computed by substituting X in the equilibrium equations.

Deformed tip cross-sections by the eight-order TE models of both configurations are shown in Figs. 12 and 13, together with variations in the shear stress components on the sheet panels. Confirming the previous remarks, the following further considerations can be made:

1) The results from the LE and MSC/NASTRAN models coincide for both structural configurations. In particular, the results from the CW model of the unribbed box are more similar to those from the solid model than to those from the solid/shell model. This is most likely due to the discontinuities in the displacement fields on the panel-stringer interfaces that affect the solid/shell model.

2) For the wing box considered, the results given by the eighth-order ($N = 8$) TE model are not sufficiently accurate. A higher-than-eighth-order TE model could be necessary to correctly detect the shear lag. However, higher-order models imply a larger number of the degrees of freedom.

3) Classical beam models and the PS approach are not able to correctly describe the wing box model without the rib.

D. Three-Bay Wing Box

The last analysis case was carried out on the three-bay wing box for which PS and BS solutions were given in Rivello's book [2]. The considered structure is shown in Fig. 14a, whereas Figs. 14b and 14c show its variations. These examples highlight the capability of the present advanced 1-D models to accurately describe the effects due to ribs and open sections. The structures consist of three wing boxes each with a length l equal to 0.5 m. The cross-section is a trapezium with height $b = 1$ m. The two webs of the spars have a thickness of 1.6×10^{-3} m, whereas $h_1 = 0.16$ m and $h_2 = 0.08$ m. The top and the bottom panels have a thickness of 0.8×10^{-3} m as well as ribs. The area of the stringers is $A_s = 8 \times 10^{-4}$ m^2. The wing is completely made of an aluminium alloy 2024, with $G/E = 0.4$. The cross-section in $y = 0$ was clamped, and a point load $F_z = 2 \times 10^4$ N was applied at $[b, 2 \times l, \frac{h_2}{2}]$.

Table 8 shows the vertical displacement values u_z and the number of degrees of freedom for each model. Results related to the CUF models are validated by an MSC/NASTRAN model built both with

Table 8 Displacement values u_z at the loaded point for each configuration of the three-bay wing box

	Full model		No-ribs case		Open mid-bay case	
	$u_z \times 10^2$, m	DOFs	$u_z \times 10^2$, m	DOFs	$u_z \times 10^2$, m	DOFs
			MSC/NASTRAN			
Solid/shell	1.412	100,026	3.051	89400	1.963	89,621
			Classical beam theories			
EBBT	0.464	495	0.464	495	0.464	495
TBT	0.477	495	0.477	495	0.477	495
			TE			
$N = 3$	0.793	1650	0.794	1650	0.873	1650
$N = 5$	1.108	3465	1.203	3465	1.500	3465
$N = 7$	1.251	5940	2.158	5940	1.745	5940
$N = 9$	1.325	9075	2.649	9075	1.836	9075
			CW			
	1.397	10,750	2.981	10,560	1.919	10,046

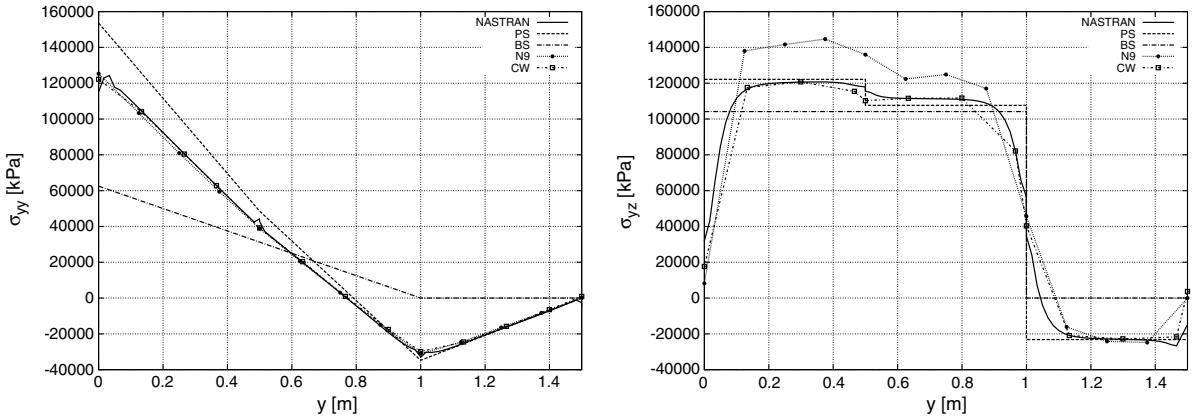

a) Bottom right spar cap; σ_{yy} at $x = b$, $z = -\frac{h_2}{2}$ b) Rear spar; σ_{yz} at $x = b$, $z = 0$

Fig. 15 Stress components distribution along the wing span. Comparison of analytical, MSC/NASTRAN and CUF models, full model of the three-bay wing box.

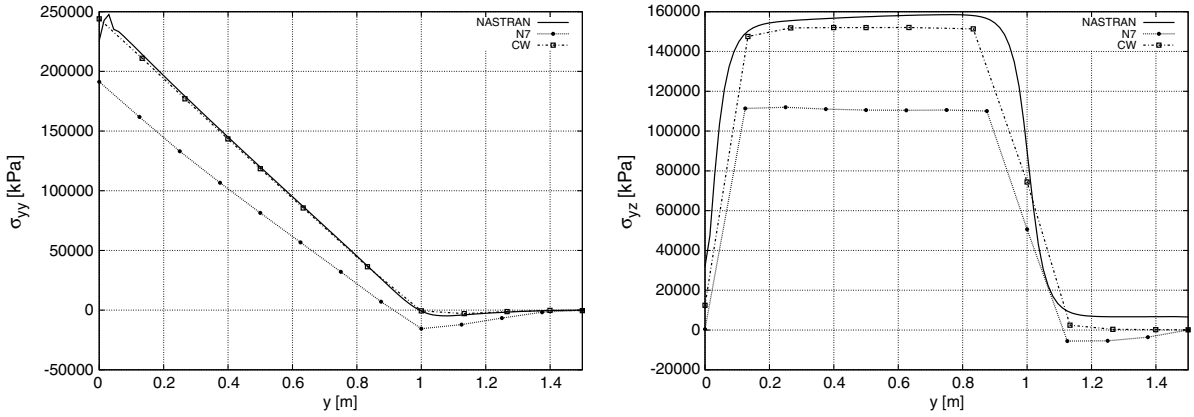

a) Bottom right spar cap; σ_{yy} at $x = b$, $z = -\frac{h_2}{2}$ b) Rear spar; σ_{yz} at $x = b$, $z = 0$

Fig. 16 Stress components distribution along the wing span. Comparison of MSC/NASTRAN and CUF models, three-bay wing box with no ribs.

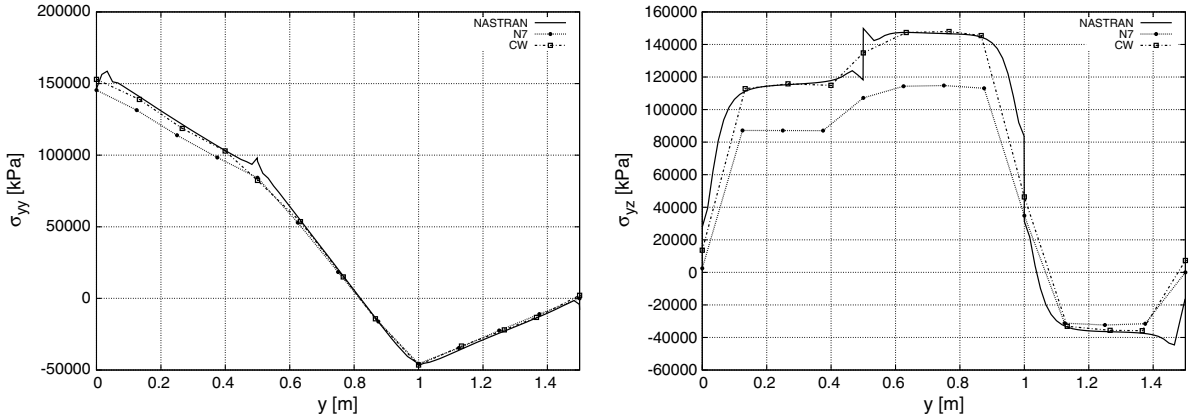

a) Bottom right spar cap; σ_{yy} at $x = b$, $z = -\frac{h_2}{2}$ b) Rear spar; σ_{yz} at $x = b$, $z = 0$

Fig. 17 Stress components distribution along the wing span. Comparison of MSC/NASTRAN and CUF models, three-bay wing box with open mid-bay.

solid and shell FE elements, as discussed in the previous analysis. The CW models were obtained by using both L4 and L9 elements, as in the rectangular wing box.

Figures 15–17 show the spanwise variation of the axial and the shear stress components for the three different configurations. BS and PS solutions are provided for the full model of the three-bay wing box for comparison. The structure has three redundancies. The PVD can be used to correct the BS solution. Let X_1, X_2, and X_3 be the redundant forces that must be added to the BS solution to obtain the true forces in the lower-left stringer at a distance of 0, l, and $2 \times l$ from the root. The redundant forces are calculated by means of the PVD. The following results hold:

$$X_1 = -36.446 \text{ N}; \qquad X_2 = -6.912 \text{ N}; \qquad X_3 = 13.908 \text{ N} \tag{32}$$

These values allow us to compute the axial forces and the shear flows for the PS method. For the complete resolution, see [2].

Table 9 Stress components σ_{yy} at $[b, l/2, -h_2/2]$ and σ_{yz} at $[b, l/2, 0]$ for each of the structural configurations of the three-bay wing box

	Full model		No-ribs case		Open mid-bay case	
Model	σ_{yy}, MPa	σ_{yz}, MPa	σ_{yy}, MPa	σ_{yz}, MPa	σ_{yy}, MPa	σ_{yz}, Pa
Solid/shell	80.598	120.730	178.147	155.368	123.841	115.351
CW LE	80.404	120.603	177.018	151.876	118.684	115.810

Finally, Table 9 reports the values of the stress components of both LE and solid/shell models. The following remarks can be made.

1) LE models match the results obtained with solid/shell models, ribs and local effects are correctly evaluated.

2) Higher-than-sixth-order TE models are required to correctly predict the cross-section deformability.

3) The PS method is quite accurate in the description of the full configuration of the three-bay wing box. Conversely, the BS method is not suitable because the structure is statically indeterminate.

V. Conclusions

This paper has considered and compared existing methods and recent approaches that exploit one-dimensional structural theories based on the unified formulation, which allows for the straightforward implementation of higher-order analysis without the need of extensive revisions of the model. Pure semimonocoque analyses along with beam assumptions have been compared to refined and component-wise models and to shell and solid solutions obtained by a commercial finite element method software.

As general guidelines and recommendations, it can be stated that Taylor expansion models should be used for global responses, such as displacements. On the other hand, component-wise models have to be adopted if local responses, such as stress and strains, are of interest. The main conclusion to be drawn is that the present component-wise analysis of reinforced shell structures appears to the authors as the most convenient way, in terms of both accuracy and computational costs, to capture the global and local (component-wise) physical behavior of wing structures. Three-dimensional finite element method analysis is required to reach the same accuracy with a number of degrees of freedom at least one order of magnitude higher than the present models. Additionally, the present component-wise approach allows the building of finite element mathematical models by only using physical surfaces; artificial lines (beam axes) and surfaces (plate/shell reference surfaces) are no longer used.

References

[1] Bruhn, E. F., *Analysis and Design of Flight Vehicle Structures*, Tri-State Offset, Cincinnati, 1973.

[2] Rivello, R. M., *Theory and Analysis of Flight Structures*, McGraw–Hill, New York, NY, 1969, p. 301.

[3] Carrera, E., *Fondamenti sul Calcolo di Strutture a Guscio Rinforzato per Veicoli Aerospaziali*, Levrotto & Bella, Turin, Italy, 2011, pp. 88, 168, 196.

[4] Cicala, P., "Sul Calcolo delle Strutture a Guscio," Part 1, *L'Aerotecnica*, Vol. 26, No. 3, 1946, pp. 138–148.

[5] Goodey, W. J., "A Stressed-Skin Problem: The Stress Distribution in the Region of Applied Loads or Constraints," *Aircraft Engineering and Aerospace Technology*, Vol. 10, No. 1, 1938, pp. 11–13. doi:10.1108/eb030262

[6] Ebner, H., and Koller, H., "Zur Berechnung des Kraftver Laufes in Versteiften Zylindershalen," *Luftfahrtforschung*, Vol. 14, 1937, pp. 607–626.

[7] Ebner, H., and Koller, H., "Ueber den Kraftverlauf in Längs und Querversteiften Scheiben," *Luftfahrtforschung*, Vol. 15, 1938, pp. 527–542.

[8] Broglio, L., "Introduzione di un Metodo Generale per il Calcolo Delle Strutture a Guscio," Istituto Poligrafico dello Stato, Rome, Monografie Scientifiche di aeronautica n. 1, 1952.

[9] Argyris, J. M., and Kelsey, S., *Energy Theorems and Structural Analysis*, Butterworths Scientific Publ., London, 1960.

[10] Satsangi, S., and Mukhopadhyay, M., "Finite Element State Analysis of Girder Bridges Having Arbitrary Platform," *International Association of Bridge and Structural Engineering*, Vol. 17, 1987, pp. 65–94.

[11] Kolli, M., and Chandrashekhara, K., "Finite Element Analysis of Stiffened Laminated Plates Under Transverse Loading," *Composite Science and Technology*, Vol. 56, No. 12, 1996, pp. 1355–1361. doi:10.1016/S0266-3538(96)00086-3

[12] Gangadhara Prusty, B., "Linear Static Analysis of Composite Hat-Stiffened Laminated Shells Using Finite Elements," *Finite Elements in Analysis and Design*, Vol. 39, No. 12, 2003, pp. 1125–1138. doi:10.1016/S0168-874X(02)00160-9

[13] Thinh, T. I., and Khoa, N. N., "Free Vibration Analysis of Stiffened Laminated Plates Using a New Stiffened Element," *Technische Mechanik*, Vol. 28, Nos. 3–4, 2008, pp. 227–236.

[14] Patel, S. N., Datta, P. K., and Seikh, A. H., "Buckling and Dynamic Instability Analysis of Stiffened Shell Panels," *Thin-Walled Structures*, Vol. 44, No. 3, 2006, pp. 321–333.

[15] Vörös, G. M., "A Special Purpose Element for Shell-Beam Systems," *Computers and Structures*, Vol. 29, No. 2, 1988, pp. 301–308. doi:10.1016/0045-7949(88)90263-5

[16] Vörös, G. M., "Finite Element Analysis of Stiffened Plates," *Periodica Polytechnica*, Vol. 51, No. 2, 2007, pp. 105–112. doi:10.3311/PPme.446

[17] Vlasov, V. Z., *Thin-Walled Elastic Beams*, National Science Foundation, Washington, DC, 1961.

[18] Abdo, M., L'Heureux, R., Pépin, F., and Kafyeke, F., "Equivalent Finite Element Wing Structural Models Used for Aerodynamics-Structures Intraction," *Proceedings of the CASI 16th Aerospace Structures and Materials Symposium*, Montreal, Quebec, April 2003.

[19] Piperni, P., Abdo, M., and Kafyeke, F., "The Building Blocks of Multi-Disciplinary Wing Design Method," *Proceedings of the CASI 50th Annual General Meeting*, Montreal, 2003.

[20] Elsayed, M. S. A., Sedaghati, R., and Abdo, M., "Accurate Stick Model Development for Static Analysis of Complex Aircraft Wing-Box Structures," *AIAA Journal*, Vol. 47, No. 9, 2009, pp. 2063–2075. doi:10.2514/1.38447

[21] Carrera, E., "Theories and Finite Elements for Multilayered, Anisotropic, Composite Plates and Shells," *Archives of Computational Methods in Engineering*, Vol. 9, No. 2, 2002, pp. 87–140. doi:10.1007/BF02736649

[22] Carrera, E., "Theories and Finite Elements for Multilayered Plates and Shells: A Unified Compact Formulation with Numerical Assessment and Benchmarking," *Archives of Computational Methods in Engineering*, Vol. 10, No. 3, 2003, pp. 216–296. doi:10.1007/BF02736224

[23] Carrera, E., and Giunta, G., "Refined Beam Theories Based on a Unified Formulation," *International Journal of Applied Mechanics*, Vol. 2, No. 1, 2010, pp. 117–143. doi:10.1142/S1758825110000500

[24] Carrera, E., Giunta, G., and Petrolo, M., *Beam Structures: Classical and Advanced Theories*, Wiley, New York, NY, 2011.

[25] Carrera, E., Giunta, G., Nali, P., and Petrolo, M., "Refined Beam Elements with Arbitrary Cross-Section Geometries," *Computers and Structures*, Vol. 88, Nos. 5–6, 2010, pp. 283–293. doi:10.1016/j.compstruc.2009.11.002

[26] Carrera, E., Petrolo, M., and Zappino, E., "Performance of CUF Approach to Analyze the Structural Behavior of Slender Bodies," *Journal of Structural Engineering*, Vol. 138, No. 2, 2012, pp. 285–297. doi:10.1061/(ASCE)ST.1943-541X.0000402

[27] Carrera, E., Petrolo, M., and Nali, P., "Unified Formulation Applied to Free Vibrations Finite Element Analysis of Beams with Arbitrary Section," *Shock and Vibrations*, Vol. 18, No. 3, 2011, pp. 485–502. doi:10.3233/SAV-2010-0528

[28] Carrera, E., Petrolo, M., and Varello, A., "Advanced Beam Formulations for Free Vibration Analysis of Conventional and Joined Wings," *Journal of Aerospace Engineering*, Vol. 25, No. 2, 2012, pp. 282–293. doi:10.1061/(ASCE)AS.1943-5525.0000130

[29] Carrera, E., and Petrolo, M., "On the Effectiveness of Higher-Order Terms in Refined Beam Theories," *Journal of Applied Mechanics*,

Vol. 78, No. 2, 2011, pp. 021013.1–021013.17.
doi:10.1115/1.4002207
[30] Carrera, E., and Petrolo, M., "Refined Beam Elements with Only Displacement Variables and Plate/Shell Capabilities," *Meccanica*, Vol. 47, No. 3, 2012, pp. 537–556.
doi:10.1007/s11012-011-9466-5
[31] Carrera, E., and Petrolo, M., "Refined One-Dimensional Formulations for Laminated Structure Analysis," *AIAA Journal*, Vol. 50, No. 1, 2012, pp. 176–189.
doi:10.2514/1.J051219
[32] Carrera, E., Maiarú, M., and Petrolo, M., "Component-Wise Analysis of Laminated Anisotropic Composites," *International Journal of Solids and Structures*, Vol. 49, No. 13, 2012, pp. 1839–1851.
doi:10.1016/j.ijsolstr.2012.03.025
[33] Euler, L., *De Curvis Elasticis*, Bousquet, Lausanne, Switzerland, 1744.
[34] Timoshenko, S. P., "On the Transverse Vibrations of Bars of Uniform Cross Section," *Philosophical Magazine*, Vol. 43, No. 253, 1922, pp. 125–131.
doi:10.1080/14786442208633855
[35] Tsai, S. W., *Composites Design*, 4th ed., Think Composites, Dayton, OH, 1988, Chap. 3.
[36] Reddy, J. N., *Mechanics of Laminated Composite Plates and Shells. Theory and Analysis*, 2nd ed., CRC Press, Boca Raton, FL, 2004, pp. 6–12.
[37] Oñate, E., *Structural Analysis with the Finite Element Method: Linear Statics*, Volume 1, Springer, Berlin, 2009, pp. 161–165.
[38] Bathe, K. J., *Finite Element Procedure*, Prentice–Hall, Upper Saddle River, NJ, 1996, p. 343.

M. W. Hyer
Associate Editor